ISPRS Journal of Photogrammetry and Remote Sensing 89 (2014) 1–12

Contents lists available at ScienceDirect

ISPRS Journal of Photogrammetry and Remote Sensing

journal homepage: www.elsevier.com/locate/isprsjprs

An improved dark object method to retrieve 500 m-resolution AOT (Aerosol Optical Thickness) image from MODIS data: A case study in the Pearl River Delta area, China

Lili Li [a,b], Jingxue Yang [c], Yunpeng Wang [a,*]

[a] State Key Laboratory of Organic Geochemistry, Guangzhou Institute of Geochemistry, Chinese Academy of Sciences, Guangzhou 510640, China
[b] University of Chinese Academy of Sciences, Beijing 100049, China
[c] Guangdong Research Institute of Water Resources and Hydropower, Guangzhou 610635, China

ARTICLE INFO

Article history:
Received 12 August 2013
Received in revised form 15 October 2013
Accepted 23 December 2013
Available online 25 January 2014

Keywords:
Aerosol
AOT retrieval
Dark object method
MODIS
Pearl River Delta

ABSTRACT

This paper presents an improved Dark Dense Vegetation (DDV) method for retrieving 500 m-resolution aerosol optical depth (AOT) based on MOD04-C005 arithmetic with the Moderate Resolution Imaging Spectroradiometer (MODIS) from the National Aeronautics and Space Administration (NASA). The improvements include change of the movement pattern of retrieval window, selection of a more suitable aerosol type, and storage of the look-up table. The method is then applied to obtain the AOT over the Pearl River Delta region (PRD). By comparing the results with the co-temporal ground sunphotometer observations in 2010, the correlation coefficient is found to be 0.794 with RMSE 0.139 and their variations remain consistent. Contrasts between model values in 2008 and MODIS AOT products in the same date also reveal a high accuracy of the improved DDV method. We also performed sensitivity tests to analyze the impacts of several parameters on apparent reflectance at different bands, and the results show that apparent reflectance is much more sensitive to surface reflectance and AOT than to elevation.

1. Introduction

Aerosols are fine particles that suspend in air in either liquid or solid form. They are often observed as dust, smoke or haze, and play a crucial role in global climatic fluctuations and regional environments (IPCC, 2007). Aerosols not only affect the climate through absorption and scattering of solar radiation (Penner et al., 1994; Myhre et al., 1998; Li et al., 2007), but also influence air quality and human health (Pope III et al., 2002).

Current aerosol measurement methods mainly include ground-based observation, numerical simulation, and satellite remote-sensing monitoring. Satellite remote-sensing can supplement the deficiency of ground-based observation by reflecting the distribution and variation of pollutants on a large scale and provide an effective way of monitoring regional aerosol distribution (Nagaraja Rao et al., 1989; Ferrare et al., 1990; Kaufman et al., 1990; Tanré and Legrand, 1991; Carlson et al., 1995; Kaufman and Tanré, 1998; Ichoku et al., 2004; Liang et al., 2006; Retalis and Sifakis, 2010). Besides, aerosol products of satellite remote-sensing are more effective for the study of urban air pollution than single-point measurement because they provide higher absolute accuracy. This method, however, has a conflict between resolution and signal-to-noise ratio (SNR); we hope to obtain Aerosol Optical Thickness (AOT) with a higher spatial resolution in the case of moderate decreases in SNR.

We tested this approach in the Pearl River Delta region (PRD) of China; a major reason for choosing this region includes the presence of complex surface features, including mountains, valleys, a coast, harbors, cities, and vegetation. In this case, aerosol products with richer spatial distribution information are of more significance than those with higher SNR and lower spatial resolution. In this research, we retrieved several 500 m-resolution AOT images of PRD from MODIS data by improving the aerosol retrieval algorithm by NASA. Then we analyzed the comparison results of retrieved AOT with field data and NASA's 10 km-resolution AOT products to validate the accuracy of the application of this new model in the area.

2. Study area and data

Located in South-Central Guangdong, China (about 21.5–24°N and 112–115.5°E), the Pearl River Delta (Fig. 1) is surrounded by mountains in the East, North and West, and faces the South China

* Corresponding author. Tel./fax: +86 20 85290197.
E-mail address: wangyp@gig.ac.cn (Y. Wang).

0924-2716/$ - see front matter © 2013 International Society for Photogrammetry and Remote Sensing, Inc. (ISPRS) Published by Elsevier B.V. All rights reserved.
http://dx.doi.org/10.1016/j.isprsjprs.2013.12.008

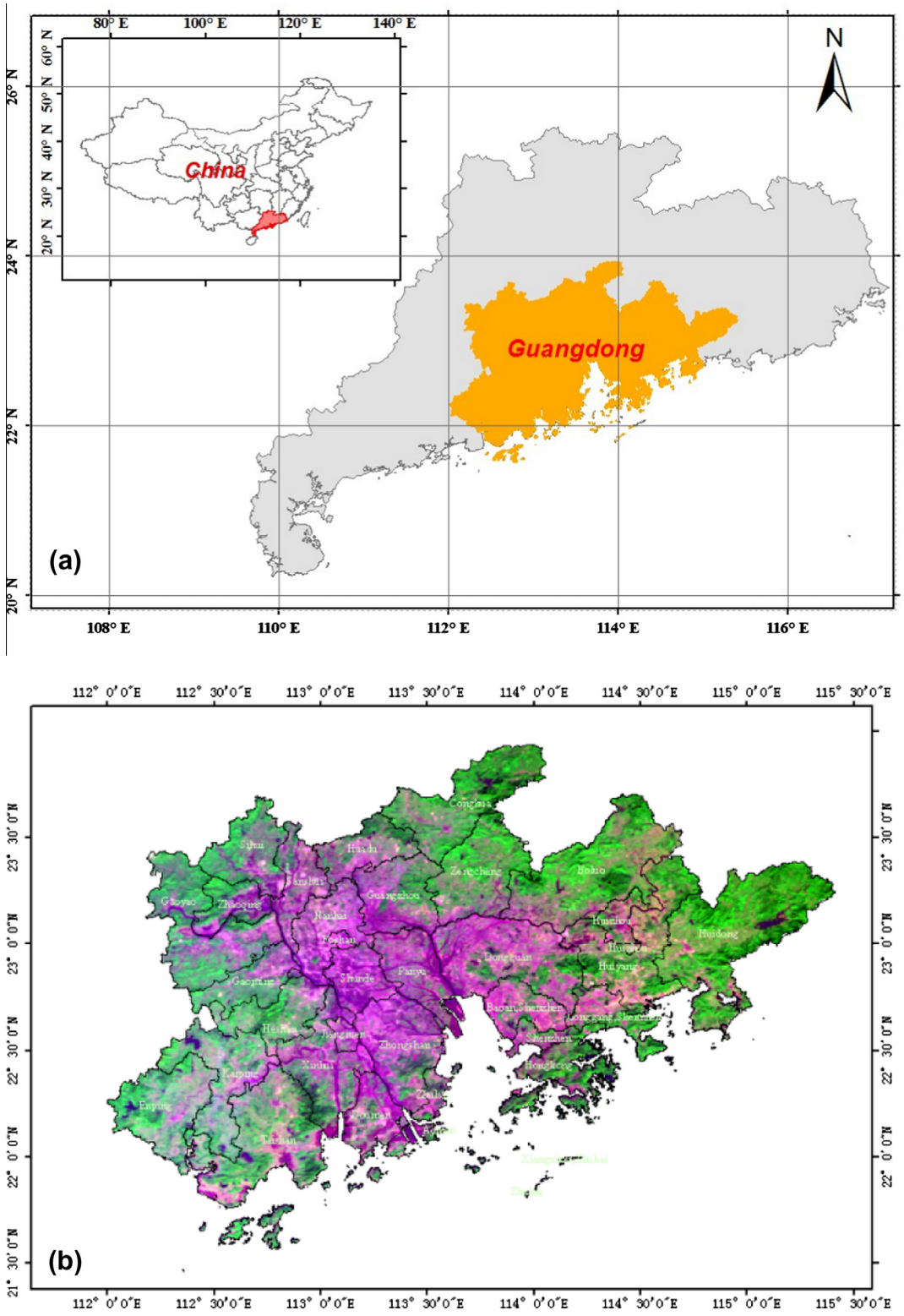

Fig. 1. Location of the Pearl River Delta in Guangdong Province, China (left) and Administrative divisions and an MODIS image of PRD (right).

Sea to the South. It has a subtropical monsoon climate, and the weather is relatively moderate with an annual average temperature of 19–21 °C. The annual average precipitation is above 1500 mm and the vegetation is mainly tropical-monsoon rainforest vegetation. Known as the most densely urbanized and populated area in Guangdong, PRD has witnessed robust economic growth, rapid industrial development, and consequently, an ever-increasing total amount of atmospheric pollutants in recent years (Lau et al., 2003; Deng et al., 2008). Hence, with hazy days in PRD increasing year-by-year, aerosol pollution has become a prominent issue and the deterioration of air quality has aroused the widespread concern of both the government and the public.

Data over PRD from MODIS (onboard Terra and Aqua satellite) used in this study were downloaded from NASA LAADS (Level 1

and Atmosphere Archive and Distribution System). They are: (1) calibrated MOD02HKM data with 500-m spatial resolution including visible, near-infrared, and mid-infrared bands in 2008 and 2010; and (2) granules of MODIS-retrieved aerosol level-2 C005 product with 10-km spatial resolution in 2008. Additionally, the Shuttle Radar Topography Mission (SRTM) data set (90 × 90 m) provided by the CGIAR Consortium for Spatial Information (http://srtm.csi.cgiar.org/) was used to identify the regional elevation.

We used a Microtops II sunphotometer from U.S Company Solar Light to obtain AOT ground measurements. MICROTOP II is a handheld sun photometer for measuring aerosol optical thickness and direct solar irradiance at five discrete wavelengths: 380 nm, 500 nm, 870 nm, 936 nm, and 1020 nm, as well as water vapor column at three wavelengths: 870 nm, 936 nm, and 1020 nm. It provides the beneficial features of high accuracy, ease-of-use, portability, and instantaneous results. The observation site of this study is on the roof a building in the Guangzhou Institute of Geochemistry (GIG) (23.15°N, 113.36°E).

3. Methodology

3.1. AOT inversion theory and algorithm

AOT retrieval through satellite remote-sensing is based on the upward reflectance ρ^* at the top of the atmosphere (TOA) observed by satellite sensors. ρ^* Is defined by:

$$\rho^* = \frac{\pi L}{\mu_s E_s} \tag{1}$$

where L is the radiance at the top of the atmosphere, E_s is the extra-terrestrial solar flux, and μ_s is the cosine of the solar zenith angle θ_s.

Assuming that the underlying surface is Lambertian and homogeneous, the relationship between ρ^* and surface reflectance ρ is shown as (Vermote et al., 1997):

$$\rho^*(\theta_s, \theta_v, \varphi) = \rho_a(\theta_s, \theta_v, \varphi) + \frac{\rho}{1-\rho S} T(\theta_s) T(\theta_v) \tag{2}$$

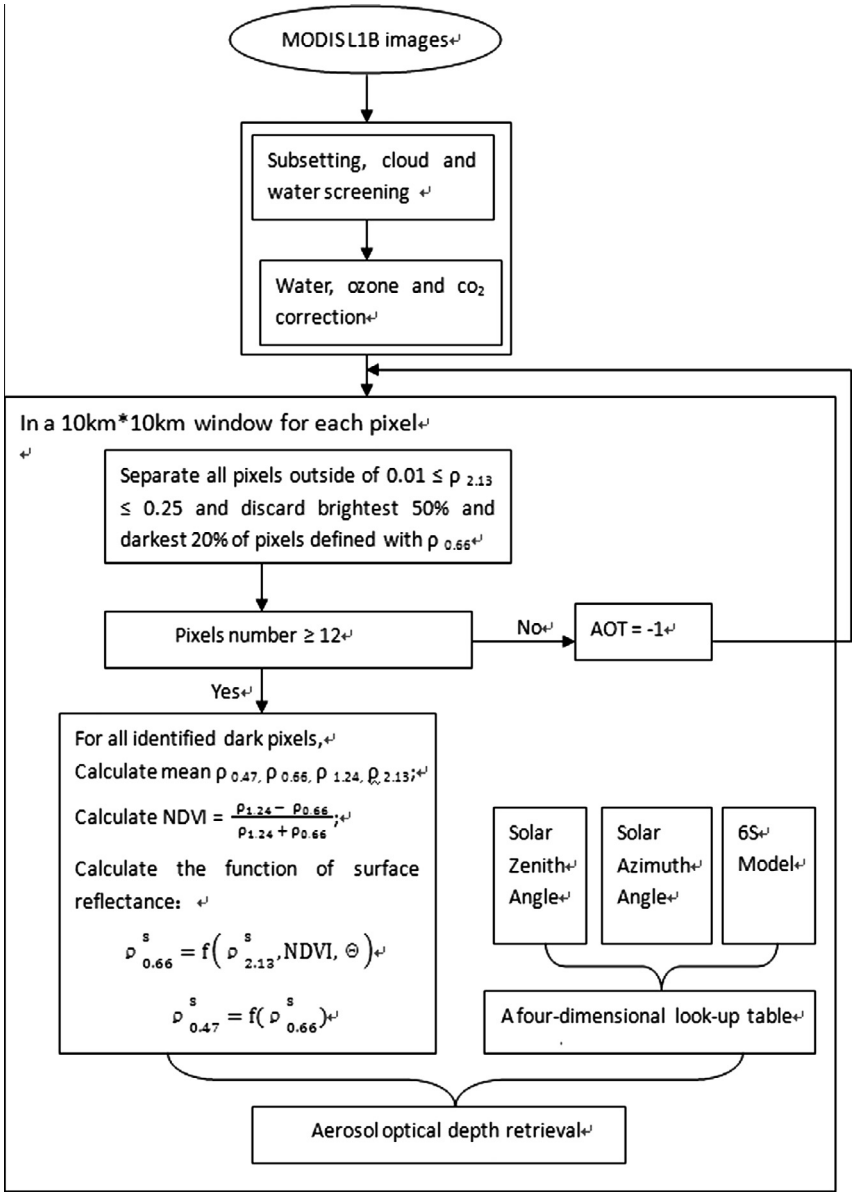

Fig. 2. The flow chart of improved aerosol retrieval showing the main processes of deriving 500 m-resolution AOTs from MODIS data.

where θ_s is solar zenith angle, θ_v is view zenith angle, φ is relative angle between the direction of propagation of scattered radiation and the incident solar direction, ρ_a is atmospheric path reflectance, $T(\theta_s)$ is upward atmospheric transmission, $T(\theta_v)$ is downward atmospheric transmission, and S is the spherical albedo of the atmosphere for illumination from below. The values of T and S depend on the single scattering albedo ω_0, aerosol optical thickness τ, and aerosol scattering phase function P.

The formulation above indicates that the apparent reflectance ρ^* is a function of both AOT and surface reflectance. Therefore, if the surface reflectance is known and the aerosol and atmospheric model are given to calculate $T(\theta_s)$, $T(\theta_s)$, S and ρ_a, then the aerosol optical thickness retrieval can be achieved.

The Dark Dense Vegetation (DDV) method, proposed by Kaufman and Sendra (Kaufman and Sendra, 1988), is based on the fact that, in the case of low surface reflectance, the 2.1-μm channel is transparent to most aerosol types so that its apparent reflectance can be seen as equal to the surface reflectance (Kaufman et al., 1997). We can then obtain the surface reflectance at the blue and red band through the established correlation between the surface reflection in the blue (0.49 μm), red (0.66 μm), and 2.1 μm, and finally retrieve AOT. The NASA V5.2 aerosol inversion algorithm is developed by Remer (Remer et al., 2005) and Levy (Levy et al., 2007) from the dark object method, revealing that the VIS vs 2.12 surface relationships have a strong dependence on both geometry and surface type.

Table 1
Gas absorption coefficients at each band.

Band	$\tau_\lambda^{H_2O}$	$\tau_\lambda^{O_3}$	$\tau_\lambda^{CO_2}$
0.47		2.432×10^{-3}	
0.55		2.957×10^{-2}	
0.66	1.543×10^{-2}	2.478×10^{-2}	
0.86	1.947×10^{-2}		
1.24	1.184×10^{-2}		4.196×10^{-4}
1.64	9.367×10^{-3}		8.260×10^{-3}
2.12	5.705×10^{-2}		2.164×10^{-2}

3.2. An improved dark object method

Aerosol products from NASA have a spatial resolution of 10 km, which is enough for global studies but obviously not adequate for studies of smaller areas, such as the Pearl River Delta area. Hence, we improved NASA's MOD04-C005 algorithm to obtain AOT distribution images with a higher spatial resolution: first, store the LUT as a four-dimensional array to enhance the operational efficiency; then, change the movement pattern of a retrieval window with 20×20 pixels for each center pixel by moving it pixel-by-pixel, so that the center pixel of the window is moved by a distance of one pixel and each will get a unique value; the improvements will be described in detail below.

The dark object method in this study includes the following steps (Fig. 2): preprocessing of MODIS data; calculation of pixel-based windows; building a four-dimensional look-up table (LUT);

Table 2
The four basic components in the aerosol model by Li et al. (2005a).

	Dust-like	Water-soluble	Oceanic	Soot
Volume component	0.13	0.7	0.15	0.005
Standard deviation	0.1	0.12	0.11	0.004

Table 3
The parameters used in setting-up the LUTs with 6S model.

Variables	Number	Value range
Channels	2	MODIS Band 1 (620–670 nm), band 3 (459–479 nm)
Elevation	3	0 m, 300 m, 800 m
Top-of-atmosphere reflectance	6	440 nm: 0.065, 0.09, 0.12, 0.15, 0.19, 0.22 660 nm: 0.0375, 0.05, 0.0625, 0.075, 0.1, 0.125
AOT	12	0.0001, 0.05, 0.1, 0.3, 0.5, 0.7, 1.0, 1.3, 1.5, 2.0, 2.5, 3

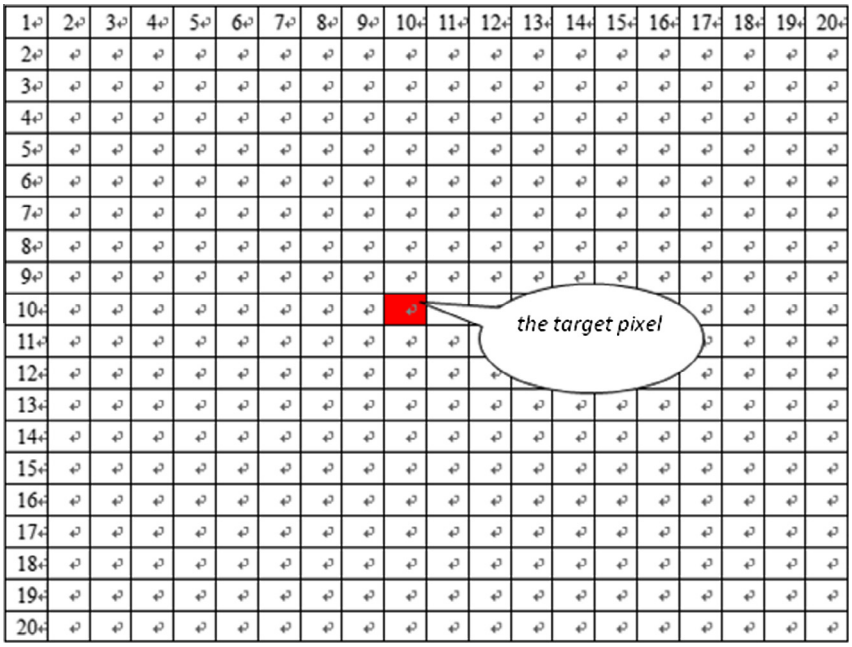

Fig. 3. Diagram of the calculation window with 20×20 pixels (10 km) opened for every pixel (500 m).

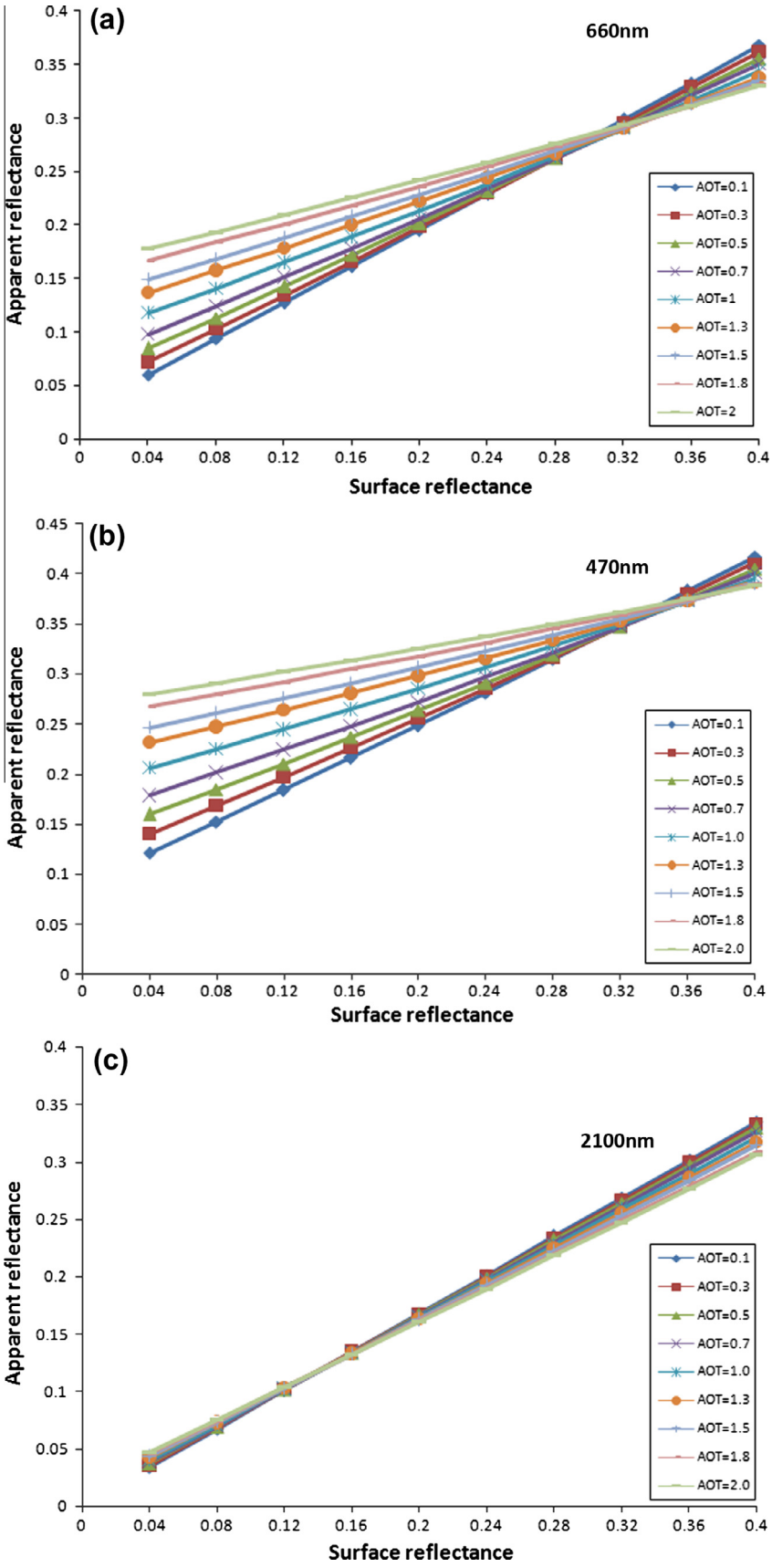

Fig. 4. Sensitivity tests of apparent reflectance to surface reflectance and AOT: (a) 660 nm; (b) 470 nm; (c) 2100 nm.

sensitivity tests of several parameters; aerosol optical thickness retrieval, and accuracy verification.

3.2.1. Pre-processing

After geometric correction, image registration, and cloud and water removal, MODIS L1B data were corrected for water, ozone, and carbon dioxide before the algorithm was applied (Remer et al., 2006; Xiao et al., 2010). The corrected apparent reflectance ρ_λ is:

$$\rho_\lambda = T_\lambda^{gas}\rho_\lambda^{L1B} \tag{3}$$

where T_λ^{gas} is the transmittance of gases and mainly includes:

$$T_\lambda^{gas} = T_\lambda^{H_2O}T_\lambda^{O_3}T_\lambda^{CO_2} \tag{4}$$

where $T_\lambda^{H_2O}$ is water transmittance; $T_\lambda^{O_3}$ is ozone transmittance; and $T_\lambda^{CO_2}$ is CO_2 transmittance. As the absorption of the gases is selective, the correction does not have to be done at all the bands:

$$T_\lambda^{H_2O} = \exp(G\tau_\lambda^{H_2O}) \tag{5}$$

$$T_\lambda^{O_3} = \exp(G\tau_\lambda^{O_3}) \tag{6}$$

$$T_\lambda^{CO_2} = \exp(G\tau_\lambda^{CO_2}) \tag{7}$$

Where $\tau_\lambda^{H_2O}$, $\tau_\lambda^{O_3}$ and $\tau_\lambda^{CO_2}$ are the water absorption coefficient, the ozone absorption coefficient, and the CO_2 absorption coefficient, respectively; G is air quality factor and is defined as:

$$G = \frac{1}{\cos\theta_s} + \frac{1}{\cos\theta_v} \tag{8}$$

where θ_s is solar zenith angle, θ_v is view zenith angle. Absorption coefficients of gases are shown in Table 1.

3.2.2. Pixel calculation

A calculation window with 20 × 20 pixels was opened for every pixel of the image as shown in Fig. 3. The reasons that the retrieval window is set to 20 × 20 pixels are: first, after the selection of dark pixels by the rules, as many as effective dark pixels are counted into the retrieval so that the center pixel of the window will get a real and reasonable value; second, choosing the same scale of window as the MOD04-C005 algorithm can facilitate the application of dark pixel masking rules of the algorithm in our study, which have been tested to be reliable for many times. The spatial resolutions of the image and the window are 500 m and 10 km, respectively. Selection of dark pixels is based on NASA's MOD04-C005 algorithm. By moving the calculation window pixel-by-pixel rather than window-by-window, each center pixel of the window

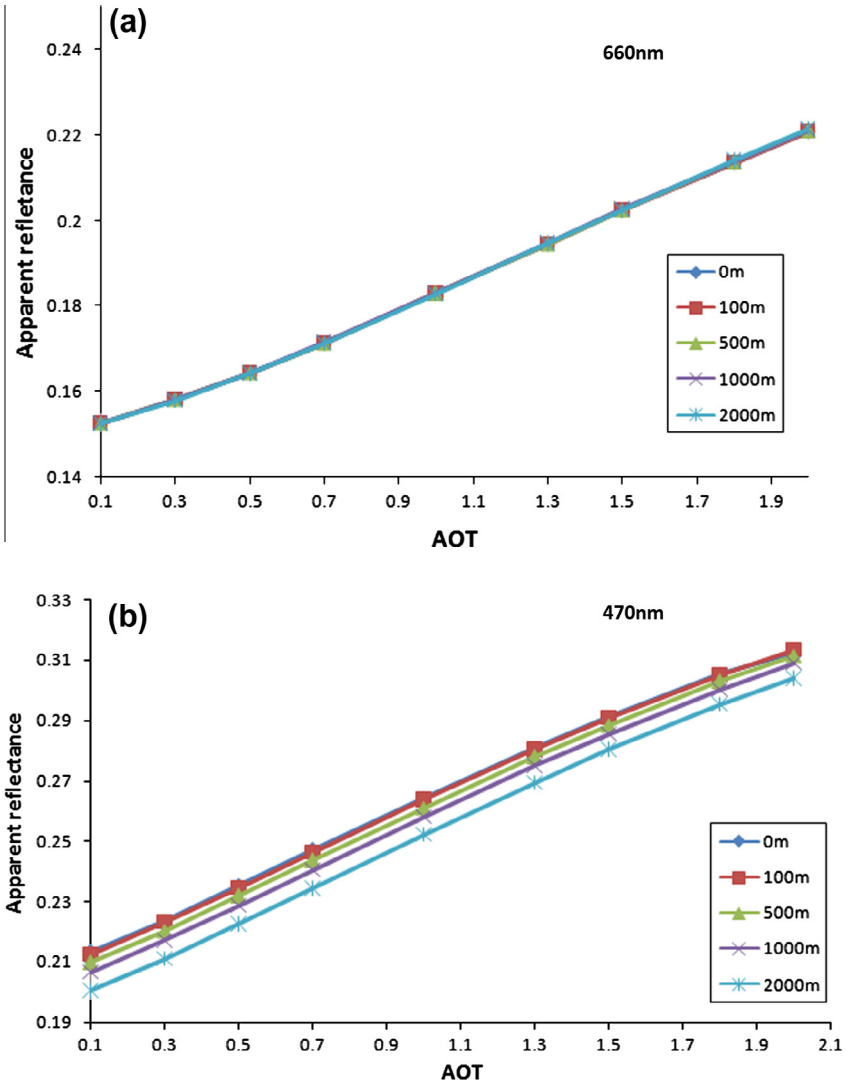

Fig. 5. Sensitivity tests of apparent reflectance to AOT at different elevations: (a) 660 nm; (b) 470 nm.

will get a unique value so that smoother and higher spatial resolution AOT maps are obtained.

The DDV method includes three steps:

First, determine the first dark pixel-sets within the range of $0.01 \leq \rho_{2.13} \leq 0.25$ and the second dark pixel-sets by discarding the pixels with the darkest 20% and brightest 50% of $\rho_{0.66}$ in the window. The intersections of the two sets are regarded as the effective dark pixels. If the number of pixels is more than 12, the next step is proceeded. Otherwise, the aerosol optical depth of the target pixel is set to −1.

Second, calculate the mean measures reflectance from the dark target pixels in the four wavelengths ($\rho_{0.47}$, $\rho_{0.66}$, $\rho_{1.24}$ and $\rho_{2.12}$).

Third, derive the surface reflectance at 0.47 and 0.66 μm ($\rho^s_{0.47}$, $\rho^s_{0.66}$) from the mean measured $\rho_{2.12}$ value using the relationships described below, which is parameterized as a function of both $NDVI_{SWIR}$ and scattering angle Θ (Remer et al., 2005; Levy et al., 2007):

$$\rho^s_{0.66} = f(\rho^s_{2.12}) = \rho^s_{2.12} * slope_{0.66/2.12} + yint_{0.66/2.12} \quad (9)$$

$$\rho^s_{0.47} = g(\rho^s_{0.66}) = \rho^s_{0.66} * slope_{0.47/0.66} + yint_{0.47/0.66} \quad (10)$$

where

$$slope_{0.66/2.12} = slope^{NDVI_{SWIR}}_{0.66/2.12} + 0.002\Theta - 0.27 \quad (11)$$

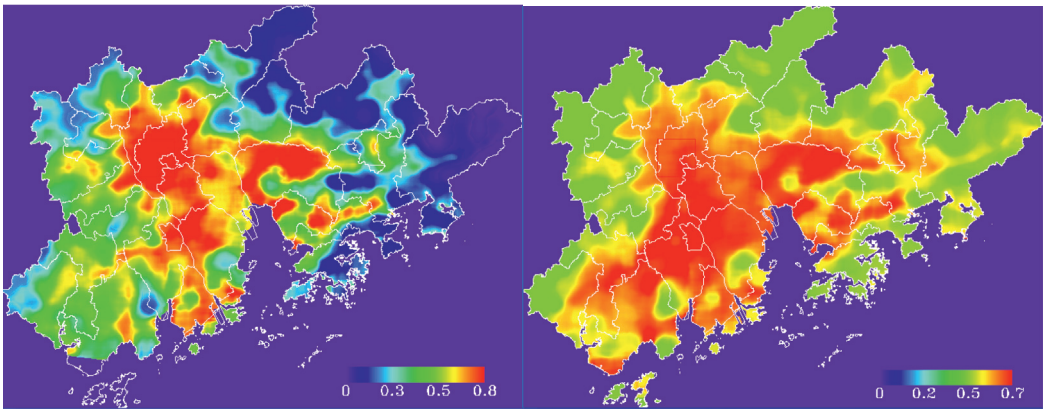

(a) November 1, 2010 (b) November 2, 2010

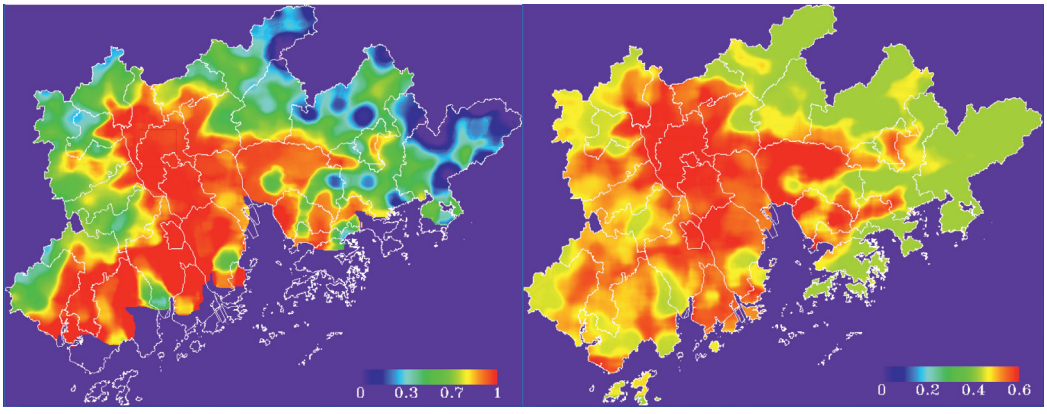

(c) November 3, 2010 (d) November 8, 2010

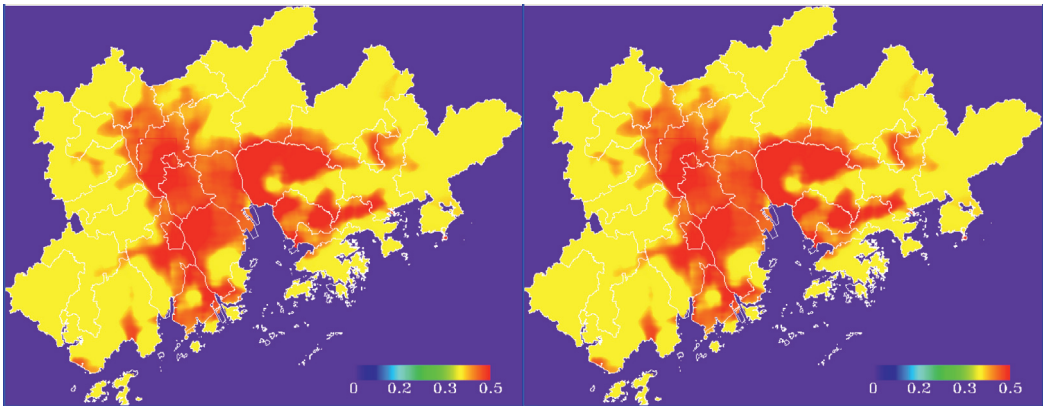

(e) December 27, 2010 (f) December 28, 2010

Fig. 6. The distribution of AOT at 550 nm derived from MODIS 500 m data from different date on November and December in 2010.

$$yint_{0.66/2.12} = -0.00025\Theta + 0.033 \quad (12)$$

$$slope_{0.47/0.66} = 0.49 \quad (13)$$

$$yint_{0.47/0.66} = 0.005 \quad (14)$$

And

$$slope_{0.66/2.12}^{NDVI_{SWIR}} = 0.48; \quad NDVI_{SWIR} < 0.25 \quad (15)$$

$$slope_{0.66/2.12}^{NDVI_{SWIR}} = 0.58; \quad NDVI_{SWIR} > 0.75 \quad (16)$$

$$slope_{0.66/2.12}^{NDVI_{SWIR}} = 0.48 + 0.2(NDVI_{SWIR} - 0.25); \quad 0.25 < NDVI_{SWIR} < 0.25 \quad (17)$$

$$\Theta = \cos^{-1}(-\cos\theta_0 \cos\theta + \sin\theta_0 \sin\theta \cos\varphi) \quad (18)$$

$$NDVI_{SWIR} = (\rho_{1.24}^m - \rho_{2.12}^m)/(\rho_{1.24}^m + \rho_{2.12}^m) \quad (19)$$

Table 4
AOT values derived from MODIS and ground-based sun photometer.

Date	MODIS-derived AOT	Observations by MICROTOPSII	Deviation
2010-11-1	0.512	0.428	0.084
2010-11-2	0.250	0.385	−0.135
2010-11-3	0.855	0.687	0.168
2010-11-8	0.325	0.328	−0.003
2010-12-27	0.047	0.209	−0.162
2010-12-28	0.455	0.329	0.126
2010-12-31	0.449	0.307	0.142

Mean absolute difference: 0.117. Correlation coefficient: 0.794. RMSE: 0.139.

3.2.3. Building a four-dimensional look-up table

The look-up table in this paper is built using 6S (Second Simulation of the Satellite Signal in the Solar Spectrum) which is a physically-basic radiative transfer-model and is not optimized on one specific satellite scene, test site, or object class. Developed from 5S (Simulation of the Satellite Signal in the Solar Spectrum), the model permits accurate simulations of near-nadir (down-looking) aircraft observations, accounting for target elevation, non-lambertian surface conditions, and new absorbing species (CH_4, N_2O, CO) (Gratzki and Gerstl, 1989; Mukai, 1990; Thome et al., 1998). The computational accuracy for Rayleigh and aerosol scattering effects has been improved by the use of state-of-the-art approximations

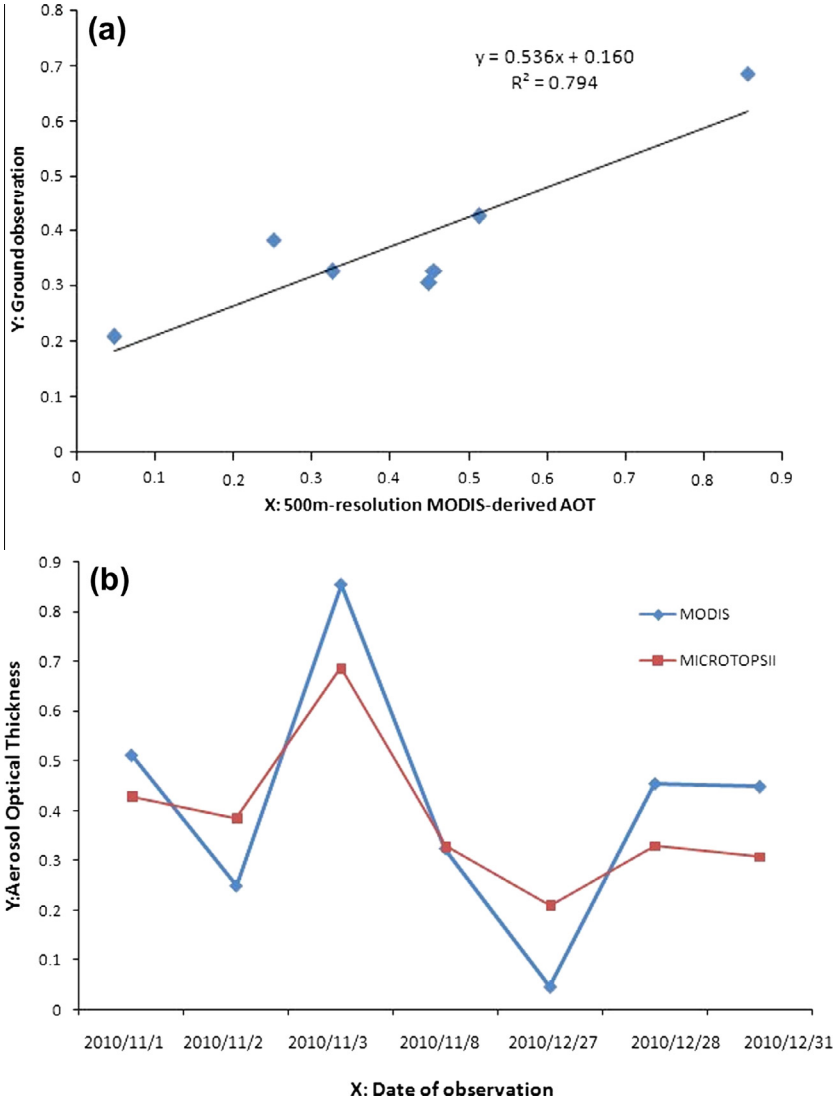

Fig. 7. Comparison between MODIS-derived 500 m AOT and ground-based sunphotometer measurements observed AOT at Guangzhou Institute of Geochemistry. (a) Is the scatter plot of MODIS-derived AOT and ground observations, with a correlation coefficient of 0.794 and RMSE 0.139. (b) Reflects the variation trends of two kinds of datasets.

and implementations of the successive order-of-scattering (SOS) algorithm (Zhao et al., 2001; Vermote et al., 2002; Kotchenova et al., 2006; Kotchenova and Vermote, 2007). The step size (resolution) used for spectral integration has been improved to 2.5 nm.

Factors affecting the atmospheric correction include geometrical conditions, the atmospheric model, the aerosol model, spectral conditions, ground reflectance, and elevation. In fact, it is difficult to obtain all parameters in any specific case, especially atmospheric data, and some standard modes are usually used to estimate the parameters. The atmosphere model in this paper was set as atmospheric water vapor amount 3.0 cm and atmospheric ozone amount 350DU. As aerosol optical thickness has the most impacts on correction results, choosing a correct aerosol type is critical. In NASA's V5.2 algorithm, the aerosol type over China is considered to be desertic or urban; for PRD, however, it is obviously coarse. Hence, we chose the aerosol type (Table 2) proposed by Li (Li et al., 2005a) which has been proved to be suitable for Hong Kong.

A look-up table was generated using the 6S radiative transfer model and the aerosol type mentioned above; the values of the parameters are shown in Table 3. Geometrical data are regarded as known inputs instead of being listed in the table so that the capacity of the LUT can be greatly reduced and the efficiency of the calculation can be enhanced. Another way that we improved operational efficiency was to store the LUT as a four-dimensional array: (FLTARR [45,13,3,2]), because it is faster to read data from arrays than from the database. The time taken to retrieve 31 800×562 AOT maps in this research was 3 min, which demonstrates a very high efficiency.

3.3. Sensitivity tests

Sensitivity of the apparent reflectance at the red, blue, and mid-infrared bands to surface reflectance and AOT determines whether it is feasible to use the DDV method for AOT retrieval. Therefore, we performed some sensitivity tests of parameters via 6S to

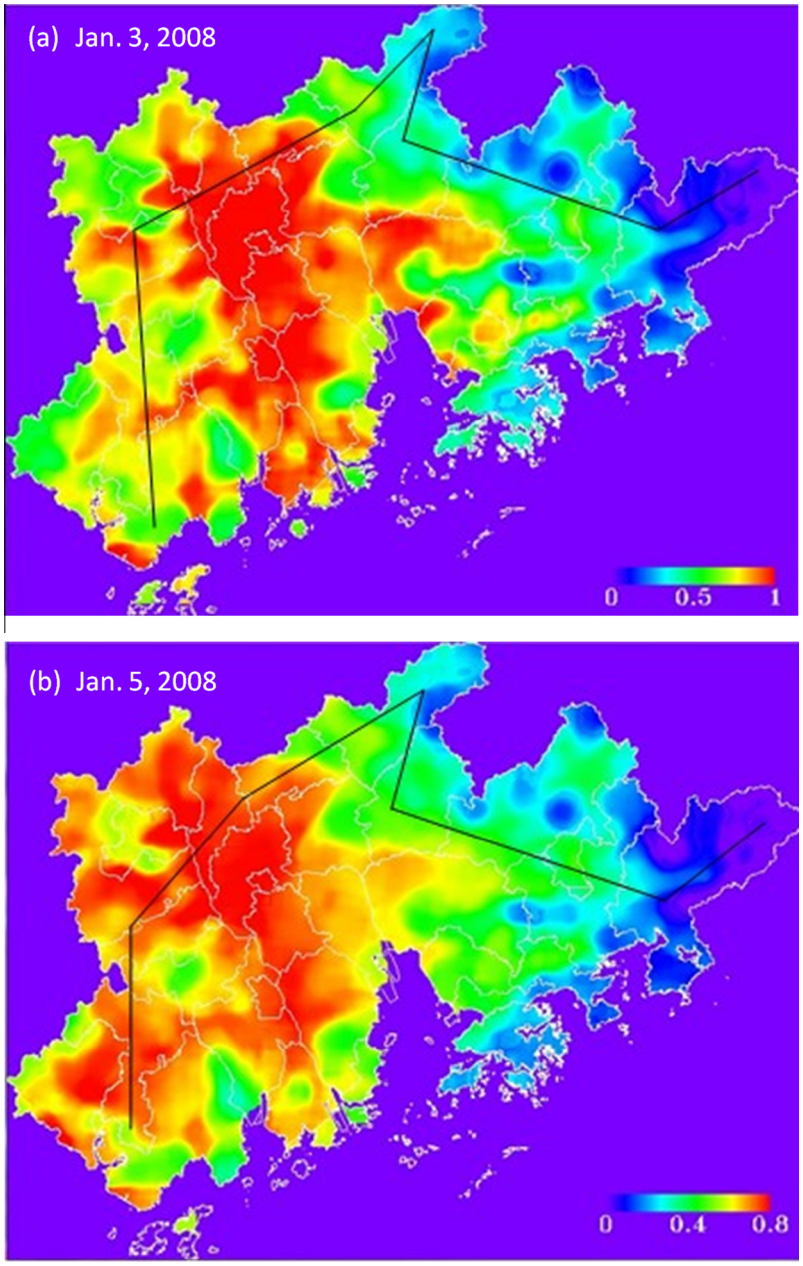

Fig. 8. The distribution of AOT at 550 nm derived from MODIS by our improved method in January, 2008: (a) January 3; (b) January 5.

identify the effects of different variables on apparent reflectance. The geometric inputs in the test are provided by selecting a location in Guangzhou on November 30, 2008 (solar zenith angle 37°, solar azimuth angle 148.07°, view zenith angle 37°, and view azimuth angle 148.07°) and the aerosol type was entered as mentioned above. Fig. 4(a) and (b) indicate that the apparent reflectance at the red and blue bands are both sensitive to AOT and surface reflectance. The apparent reflectance increases with increasing surface albedo, while it increases first and then decreases with increasing AOT; there also exists a threshold point which lies in the surface reflectance of 0.31 at the red channel and 0.34 at the blue channel. An insensitivity of the apparent reflectance of the mid-infrared band to AOT variations when the surface reflectance is less than 0.2 is demonstrated in Fig. 4(c), which meets the prerequisite of the dark object method. Fig. 4 also shows that the aerosol type that we selected is applicable to the PRD region.

Owing to correlations between the atmospheric molecules, as well as other minor components and elevation, the retrieval results are also influenced by elevation. Fig. 5 reflects the relationship between apparent reflectance and AOT at different heights. It is obvious that the impact of elevation on 470 nm channel is greater than 660 nm; however, this impact is much smaller compared with aerosols, mainly because the effects of the atmospheric molecular-scattering caused by elevation are much less than those caused by aerosols.

4. Results validation and discussion

Fig. 6(a)–(f) are parts of the retrieved 500 m-resolution AOT at 550 nm from MODIS in November and December, 2010 through our improved DDV method.

Comparisons of the results and ground observations at the same site and same date were then made for verification (Table 4 and Fig. 7). Data for November 1, 2, 3, 8 and December 27, 28, and 31 were selected because of good weather, cloudless skies, and corresponding measurements at 500 nm by MICROTOP II. As shown in Fig. 7(a), the accuracy of AOTs in the PRD retrieved from MODIS via the improved dark object method is within the expected range

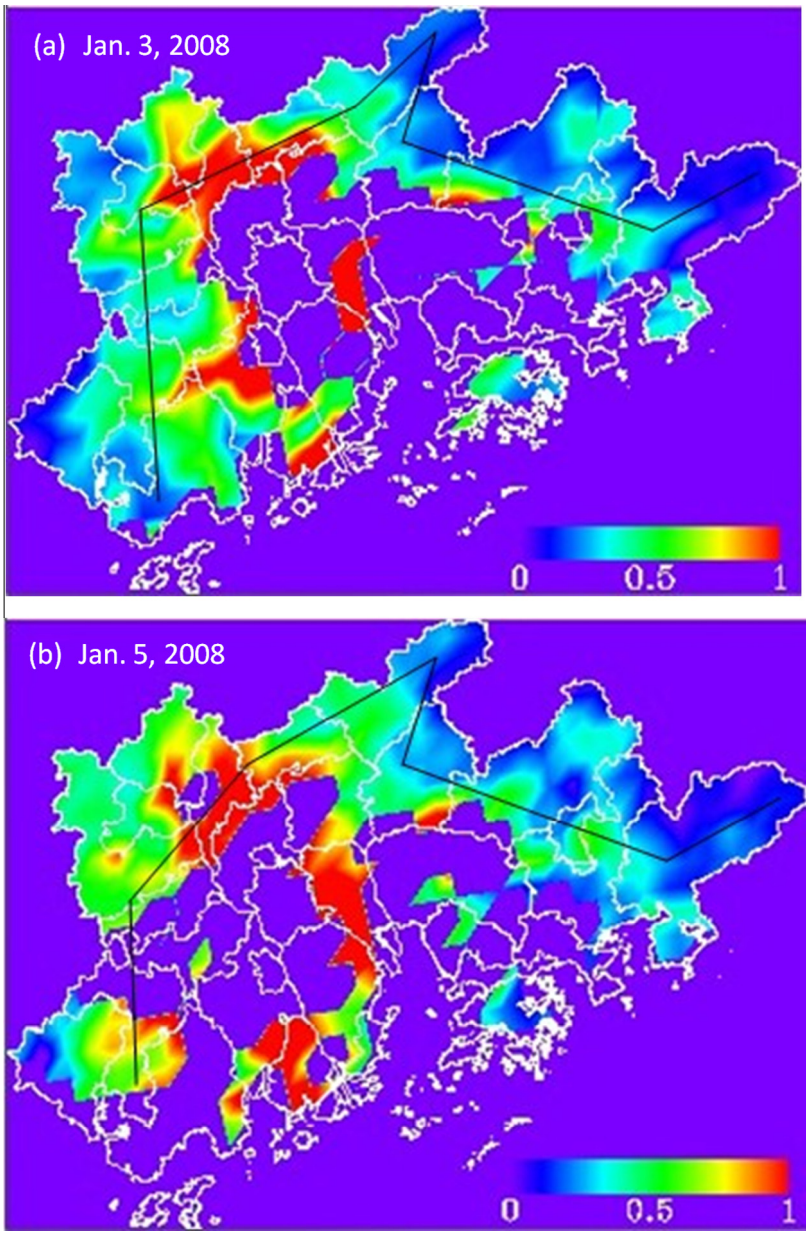

Fig. 9. MODIS aerosol products by NASA in January, 2008: (a) January 3; (b) January 5.

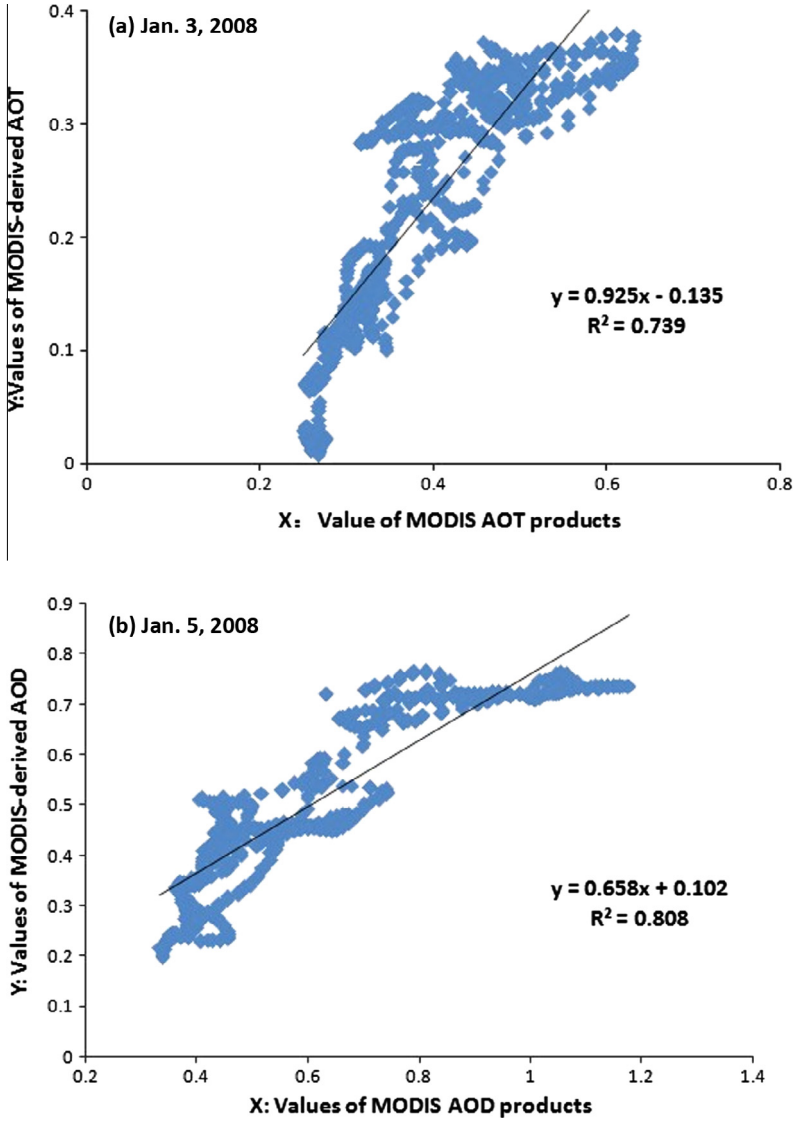

Fig. 10. The comparison between our derived 500 m AOT and 10 km AOT products with correlation coefficient of 0.5532 on January 3 and 0.7639 on January 5.

with a correlation coefficient 0.794 and RMSE 0.139; this is close to that of AOT retrievals in Hong Kong by Li (Li et al., 2005b) with RMSE 0.12. It is also found in Fig. 7(b) that MODIS-derived results generally show a positive bias from the observations at high values of optical thickness, which has been confirmed in other research (Chu et al., 2002; Levy et al., 2005; Mi et al., 2007). The reasons for this may be a possible instrument calibration issue or improper representation of surface reflectance in a systematic way at certain locations and seasons. But the changing trends of model values and observations are similar, suggesting that the relative values of retrieved AOT over PRD are reliable even though the absolute data may not be perfectly accurate.

Then we compared our 500 m-resolution retrieved AOT (Fig. 8) with 10 km AOT products released by NASA, which were derived by using MOD04-C005 algorithm (Fig. 9) on January 1 and 3, 2008, as the algorithm is the base of our study. The results reveal that AOT maps in PRD produced by our algorithm are much smoother and cover more extensive value ranges with fewer null values in cloudless weather. Several Regions of Interest (ROIs), including areas of high values, medium values and low values, were selected in the black line in the maps.

Fig. 10 is two-dimensional scatterplots of the black line areas of AOT products and MODIS-derived AOT in Fig. 9. Strips of points appear in the plots because the spatial resolution of AOT products is much coarser than 500 m derived AOTs and one pixel in AOT products equals 20×20 pixels in derived AOTs. Results of our model are shown to have a high correlation with MODIS AOT product (0.739 and 0.808, respectively), but most of the values are lower than product values (the difference between values of two kinds of products is about 0.15 to 0.2), mainly due to the different types of aerosol used in the model: desertic or urban in NASA's algorithm and specific volume components in our method. As resizing the 10 km resolution image is not reasonable for edge pixels, our method is probably more proper for the study of AOT in smaller regions.

5. Conclusion

Several improvements on the MOD04-C005 algorithm are made in this paper and mainly include: (a) building a window with 20×20 pixels for each center pixel, calculating the AOT value of the window as that of the target pixel and then moving the window pixel-by-pixel; (b) choosing an aerosol type more suitable for the Pearl River Delta region; and (c) storing the look-up table as a four-dimensional array to improve the operational efficiency

of the algorithm. These improvements can also be applied in other regions, and only modification is to change the input aerosol type suitable to the local conditions.

AOT maps with 500 m-resolution in PRD are obtained by using the improved dark object method, resulting in greatly improved spatial resolution compared to MODIS AOT products. The accuracy of our algorithm is validated by ground observations: the correlation coefficient is 0.794 and RMSE is about 0.139. Though model values are generally higher than observations at low optical thickness, they present similar change trends.

The comparison between MODIS derived AOTs and 10 km MODIS AOT products shows a high correlation with correlation coefficient R^2 about 0.75 to 0.8, but the retrieved values are lower than the products with the difference being about 0.15 to 0.2, which may be a result of the different aerosol types used in the algorithm.

We also performed sensitivity tests of some parameters via direct calculation in 6S and found that the apparent reflectance at the red and the blue band are both sensitive to AOT and surface reflectance. There is a positive relationship between apparent reflectance and surface albedo, and an inflection point exists in the variations of apparent reflectance with AOT (0.31 at the red band and 0.34 at the blue band). Elevation also has an impact on 470 nm channel, but the impact is much smaller when compared with aerosols.

Acknowledgments

China National Key Technology R&D Program (2012BAH32B03), China National 863 Program (2006AA06A306) and Guangdong NSF (S2013010014097) are acknowledged for financial supports. We also thank the NASA Earth System for the MODIS products. Mr. Jake Carpenter of Beverly Hills English is greatly acknowledged for his help for improving the English of this manuscript. This is contribution No. SKLOG2013A01 from SKLOG and No. IS-1804 from GIGCAS.

References

Carlson, T.N. et al., 1995. A new look at the simplified method for Remote-Sensing of daily evapotranspiration. Remote Sens. Environ. 54 (2), 161–167.
Chu, D.A. et al., 2002. Validation of MODIS aerosol optical depth retrieval over land. Geophys. Res. Lett. 29 (12), 8007.
Deng, X.J. et al., 2008. Long-term trend of visibility and its characterizations in the Pearl River Delta (PRD) region, China. Atmos. Environ. 42 (7), 1424–1435.
Ferrare, R.A. et al., 1990. Satellite Measurements of large-Scale air-pollution: measurements of forest fire smoke. J. Geophys. Res.: Atmos. 95 (D7), 9911–9925.
Gratzki, A., Gerstl, S.A.W., 1989. Sensitivity of an atmospheric correction algorithm for non-lambertian vegetation surfaces to atmospheric parameters. Geosci. Remote Sens., IEEE Trans. 27 (3), 326–331.
Ichoku, C. et al., 2004. Global aerosol remote sensing from MODIS. Adv. Space Res. 34 (4), 820–827.
IPCC, 2007. Climate change 2007: the physical science basis. Agenda 6 (07).
Kaufman, Y.J., Sendra, C., 1988. Algorithm for automatic atmospheric corrections to visible and near-IR satellite imagery. Int. J. Remote Sens. 9 (8), 1357–1381.
Kaufman, Y.J. et al., 1990. Satellite measurements of large-scale air pollution: methods. J. Geophys. Res. 95 (D7), 9895–9909.
Kaufman, Y.J. et al., 1997. The MODIS 2.1-μm channel-correlation with visible reflectance for use in remote sensing of aerosol. Geosci. Remote Sens. IEEE Trans. 35 (5), 1286–1298.
Kaufman, Y.J., Tanré, D., 1998. Algorithm for remote sensing of tropospheric aerosol from MODIS. NASA MODIS Algorithm Theoretical Basis Document, Goddard Space Flight Center 85.
Kotchenova, S.Y. et al., 2006. Validation of a vector version of the 6S radiative transfer code for atmospheric correction of satellite data. Part I: Path radiance. Appl. Opt. 45 (26), 6762–6774.
Kotchenova, S.Y., Vermote, E.F., 2007. Validation of a vector version of the 6S radiative transfer code for atmospheric correction of satellite data. Part II. Homogeneous Lambertian and anisotropic surfaces. Appl. Opt. 46 (20), 4455–4464.
Lau, K.H. et al., 2003. A new way of using MODIS data to study air pollution over Hong Kong and the Pearl River Delta. Proc. Int. Soc. Opt. Eng. 4891, 105–114.
Levy, R.C. et al., 2005. Evaluation of the MODIS aerosol retrievals over ocean and land during CLAMS. J. Atmos. Sci. 62 (4), 974–992.
Levy, R.C. et al., 2007. Second-generation operational algorithm: retrieval of aerosol properties over land from inversion of Moderate Resolution Imaging Spectroradiometer spectral reflectance. J. Geophys. Res.: Atmos. 112 (D13).
Li, C.C. et al., 2005a. Remote sensing of high spatial resolution aerosol optical depth with MODIS Data over Hong Kong. Chinese J. Atmos. Sci. 29 (3), 335–342.
Li, C.C. et al., 2005b. Retrieval, validation, and application of the 1-km aerosol optical depth from MODIS measurements over Hong Kong. Geosci. Remote Sens. IEEE Trans. 43 (11), 2650–2658.
Li, Z.Q. et al., 2007. Aerosol optical properties and their radiative effects in northern China. J. Geophys. Res.: Atmos. 112 (D22).
Liang, S. et al., 2006. Improved estimation of aerosol optical depth from MODIS imagery over land surfaces. Remote Sens. Environ. 104 (4), 416–425.
Mi, W. et al., 2007. Evaluation of the moderate resolution imaging spectroradiometer aerosol products at two aerosol robotic network stations in China. J. Geophys. Res. 112 (D22), D22S08.
Mukai, S., 1990. Atmospheric correction of Remote-Sensing images of the ocean based on multiple-scattering calculations. Geosci. Remote Sens. IEEE Trans. 28 (4), 696–702.
Myhre, G. et al., 1998. Estimation of the direct radiative forcing due to sulfate and soot aerosols. Tellus B 50 (5), 463–477.
Nagaraja Rao, C.R. et al., 1989. Remote sensing of aerosols over the oceans using AVHRR data Theory, practice and applications. Int. J. Remote Sens. 10 (4–5), 743–749.
Penner, J.E. et al., 1994. Quantifying and minimizing uncertainty of climate forcing by anthropogenic aerosols. Bull. Am. Meteorol. Soc. 75 (3), 375–400.
Pope III, C.A. et al., 2002. Lung cancer, cardiopulmonary mortality, and long-term exposure to fine particulate air pollution. JAMA J. Am. Med. Assoc. 287 (9), 1132–1141.
Remer, L.A. et al., 2005. The MODIS aerosol algorithm, products, and validation. J. Atmos. Sci. 62 (4), 947–973.
Remer, L.A., et al., 2006. Algorithm for remote sensing of tropospheric aerosol from MODIS: Collection 005. National Aeronautics and Space Administration.
Retalis, A., Sifakis, N., 2010. Urban aerosol mapping over Athens using the differential textural analysis (DTA) algorithm on MERIS-ENVISAT data. ISPRS J. Photogram. Remote Sens. 65 (1), 17–25.
Tanré, D., Legrand, M., 1991. On the satellite retrieval of Saharan dust optical thickness over land: two different approaches. J. Geophys. Res. 96 (D3), 5221–5227.
Thome, K. et al., 1998. Atmospheric correction of ASTER. Geosci. Remote Sens. IEEE Trans. 36 (4), 1199–1211.
Vermote, E.F. et al., 1997. Second simulation of the satellite signal in the solar spectrum, 6S: an overview. Geosci. Remote Sens. IEEE Trans. 35 (3), 675–686.
Vermote, E.F. et al., 2002. Atmospheric correction of MODIS data in the visible to middle infrared: first results. Remote Sens. Environ. 83 (1), 97–111.
Xiao, Z.Y. et al., 2010. The retrieval of aerosol optical thickness with high spatial resolution using MODIS data over Guangzhou. China Environ. Sci. 30 (5), 577–584.
Zhao, W. et al., 2001. Atmospheric and spectral corrections for estimating surface albedo from satellite data using 6S code. Remote Sens. Environ. 76 (2), 202–212.